A composite time integration scheme for dynamic adhesion and its application to gecko spatula peeling

Sachin S. Gautam[1]

Department of Mechanical Engineering
Indian Institute of Technology Guwahati, 781 039, Assam, India

Roger A. Sauer

Graduate School AICES, RWTH Aachen University, Templergraben 55, 52056 Aachen, Germany

Abstract: Simulation of dynamic adhesive peeling problems at small scales has attracted little attention so far. These problems are characterized by a highly nonlinear response. Accurate and stable time integration schemes are required for simulation of dynamic peeling problems. In the present work, a composite time integration scheme is proposed for the simulation of dynamic adhesive peeling problems. It is shown through numerical examples that the proposed scheme remains stable and also has some gain in accuracy. The performance of the scheme is compared with two collocation-based schemes, i.e. Newmark scheme and Bathe composite scheme. It is shown that the proposed scheme and Bathe composite scheme perform equally. However, the proposed scheme adds very little to the computational cost of Newmark scheme. Through a numerical simulation of the peeling of a gecko spatula from a rigid substrate it is shown that the proposed scheme and the Bathe composite scheme are able to simulate the complete peeling process for given time step whereas the Newmark scheme diverges. It is also shown that the maximum pull-off force is within the range reported in the literature.

Keywords: Time integration; collocation-based schemes; composite scheme; contact mechanics; peeling; gecko adhesion.

1 Introduction

The focus of the current work is on modeling and simulation of peeling problems that occur at small length scales by taking into account dynamic effects. Dynamic peeling simulation problems at such small scales belong to the class of contact problems where the contact forces can be derived from a potential formulation like those based on Van der Waals forces. An example is the adhesion and peeling of a gecko spatula [Sauer (2010)]. These problems are highly nonlinear in nature. Simulation of these problem requires accurate time integration schemes. To the best of authors knowledge, very little literature exists on dynamic simulation of peeling problems at small scales, see e.g. [Sauer (2010)].

A number of time integration schemes exist in the literature which can be classified into two different categories: *collocation-based schemes* and *energy-momentum conserving schemes* [Krenk (2009)]. In

---

[1]Corresponding author, email: ssg@iitg.ernet.in
[2]This pdf is a personal version of an article whose final publication is available at http://www.worldscientific.com/

collocation-based schemes, the equation of motion is satisfied at selected points in the time interval. In contrast, for energy-momentum-conserving schemes, the equation of motion is explicitly integrated over the time interval. The Newmark scheme [Newmark (1959)], which is a parameter-based collocation based scheme, may induce significant errors in the numerical solution which then leads to divergence of the numerical solution in case of nonlinear problems. Recently, a parameter-free collocation-based composite time integration scheme has been proposed by Bathe and co-workers [Bathe (2007); Bathe and Baig (2005)] with the objective to conserve energy. In a later work, see [Bathe and Noh (2012)], it is shown that the scheme dissipates energy for spurious higher modes. Alternatively, *energy-momentum conserving schemes* have been developed with the idea of conserving properties of the underlying problem i.e., momentum and energy. Energy-momentum conserving schemes were first applied to elastodynamics by Simo and Tarnow (1992). They presented a new methodology for the construction of time integration algorithms, called energy-momentum conserving algorithms (EMCA), that inherit, by design, the conservation laws of momentum and energy. Later, Betsch and Steinmann (2001) used a non-standard quadrature formula, based on the discrete gradient method of Gonzalez (1996), for studying the energy conservation in nonlinear elastodynamics. Recently, Hesch and Betsch [Hesch and Betsch (2009, 2010)] have developed a new energy-momentum conserving scheme by extending the discrete gradient method of Gonzalez (1996) and the one-step method of Betsch and Steinmann (2001) for contact-impact problems using the mortar finite element method.

Recently, Gautam and Sauer (2013) have proposed an energy-momentum conserving time integration scheme for dynamic adhesive contact problems based on the concept of the discrete gradient. This scheme leads to major accuracy gains in conserving the energy over the collocation based schemes. However, the methods based on discrete gradient approach suffer from some drawbacks. First, the evaluation of the discrete gradient, specially for the bulk, requires large computational time. Also, the discrete gradient is specific to the material properties through strain energy density function. This restricts the application of a scheme based on discrete gradient to different materials. Hence, application of methods based on the discrete gradient approach is mostly restricted to small scale problems. Instead, various collocation-based schemes like Newmark scheme [Newmark (1959)] and Bathe's composite scheme [Bathe (2007); Bathe and Baig (2005)] are still applied which ensure reasonable accuracy without severely affecting the computational time. The objective of the present work is to propose a composite time integration scheme, which does not suffer from the drawbacks mentioned previously i.e., it can be applied to general materials and should not affect the computational time without affecting the accuracy. Hence, in the present work, a composite time integration scheme is proposed for dynamic adhesive contact problems which incorporates the intended objectives. The performance and accuracy of the proposed scheme is compared with two class of collocation-based schemes i.e. the parameter-based Newmark scheme [Newmark (1959)] and the parameter-free Bathe's composite scheme [Bathe (2007); Bathe and Baig (2005)] through two simple numerical examples i.e., interaction of a deformable ball with a rigid surface and peeling of a deformable strip from a rigid substrate. It is shown that there is gain in accuracy compared to collocation-based schemes and also the computational cost in only slightly higher compared to Newmark scheme. Finally, the peeling of a gecko spatula pad from a rigid surface is simulated using the proposed scheme and its performance evaluated in comparison with collocation-based schemes. In particular, the computational time required for each scheme is also evaluated.

The remainder of this paper is structured as follows: Section 2 provides an overview of the adhesion model used to describe adhesive contact between deformable bodies and also presents the finite element formulation. Section 3 first presents a brief discussion on the implementation of the collocation based schemes proposed by Newmark [Newmark (1959)] and Bathe and coworkers [Bathe (2007); Bathe and Baig (2005)]. Then, the proposed composite time integration scheme is presented. In Section 4, results of two numerical examples: dynamic interaction of a deformable ball with a rigid surface and peeling of a deformable strip from a rigid substrate are presented. Numerical results of dynamic peeling of a gecko spatula from rigid surface are presented in the end. Section 5 concludes this paper.

2 Formulation

In this section, we first present the adhesion formulation employed in the present work followed by the finite element formulation.

2.1 Adhesion formulation

Here, a brief overview of the adhesion formulation considered in the present work is presented which is suitable to describe a large class of interaction mechanisms like classical contact with penalty and barrier formulations, physical interaction formulations like cohesive zone models as well as electrostatic, gravitation, and Van der Waals interactions, see [Sauer and Lorenzis (2013)]. According to the model, the interaction between two deformable bodies $\mathcal{B}_k$ ($k = 1, 2$) is described by the contact interaction energy

$$\Pi_c = \int_{\partial \mathcal{B}_k} \beta_k^s \Phi_\ell \, da_k \, , \tag{1}$$

where β_k^s is the current surface density at $x_k \in \partial \mathcal{B}_k$, defined as the number of interacting particles per current surface area, and Φ_ℓ denotes the interaction potential between a particle at x_k and the neighboring body $\mathcal{B}_\ell$ ($\ell \neq k$). The potential Φ_ℓ depends on the signed distance r_s between point x_k and surface $\partial \mathcal{B}_\ell$ i.e.,

$$r_s(x_k) := (x_k - x_p) \cdot n_p \, , \tag{2}$$

where x_p is the closest projection point of x_k on $\partial \mathcal{B}_\ell$ and n_p is the corresponding surface normal. Alternatively, Eq. (1) is expressed in the reference configuration as

$$\Pi_c = \int_{\partial \mathcal{B}_{0k}} \beta_{0k}^s \Phi_\ell \, dA_k \, , \tag{3}$$

where $\mathcal{B}_{0k}$ ($k = 1, 2$) denotes the reference configuration of the body k and β_{0k}^s is the reference surface density, expressed as the number of interacting particles per reference surface area. Here, we consider the number of surface particles to be conserved during deformation such that

$$\beta_k^s \, da_k = \beta_{0k}^s \, dA_k = \text{const.} \tag{4}$$

This assumption is reasonable for solids. The variation of Π_c, due to variations of configuration x_k, denoted $\delta x_k = \delta \varphi_k$, now becomes

$$\delta \Pi_{c,k} = \int_{\partial \mathcal{B}_{0k}} \beta_{0k}^s \frac{\partial \Phi_\ell}{\partial x_k} \cdot \delta \varphi_k \, dA_k = \int_{\partial \mathcal{B}_k} \beta_k^s \frac{\partial \Phi_\ell}{\partial x_k} \cdot \delta \varphi_k \, da_k \, . \tag{5}$$

In this equation, we can identify the interaction force

$$F_k := -\frac{\partial \Phi_\ell}{\partial x_k} \, . \tag{6}$$

The surface traction, in the current or reference configuration, is then identified as

$$t_k = \beta_k^s F_k, \qquad \text{or} \qquad T_k = \beta_{0k}^s F_k \, . \tag{7}$$

For suitable definitions of Φ_ℓ, one can consider various contact formulations [Sauer and Lorenzis (2013)]. In the present work, we focus on van der Waals adhesion for which we have

$$\Phi_\ell := \frac{\Phi_0}{J_{s\ell}} \left[\frac{1}{360} \left(\frac{r_0}{r_s} \right)^8 - \frac{1}{6} \left(\frac{r_0}{r_s} \right)^2 \right] \, , \qquad r_s > 0 \, . \tag{8}$$

Here, Φ_0 and r_0 are model constants and $J_{s\ell} = da_k/dA_k = \beta_{0k}^s/\beta_k^s$ characterizes the surface deformation. The corresponding traction, using Eqs. (6) and (7), is given by

$$T_k = \frac{T_0}{J_{s\ell}} \left[\frac{1}{45} \left(\frac{r_0}{r_s} \right)^9 - \frac{1}{3} \left(\frac{r_0}{r_s} \right)^3 \right] n_p \; . \tag{9}$$

Here, T_0, which describes the adhesive strength, is proportional to Hamaker's constant A_H [Israelachvili (1991)].

Remark:

1. In the present work, only frictionless normal contact is considered.

2. If one of the bodies is rigid for e.g., if $\mathcal{B}_\ell$ is rigid, then $J_{s\ell} = 1$.

3. It should be noted that although the contact potential (Eq. 8) and traction (Eq. 9) are smooth functions of distance and time, spatial, and temporal discretization can lead to nonsmooth functions. This will require spatial and temporal adaptivity to approximate smooth behavior.

2.2 Finite element formulation

The expression of the finite element equations associated with the contact traction given by (9) is now simple to derive. For a general, three-dimensional finite element discretization of bodies $\mathcal{B}_k$ ($k = 1, 2$), the expression for the equation of motion for dynamic problem is given by

$$\mathbf{M}\ddot{\mathbf{u}} + \mathbf{f}_{int} + \mathbf{f}_c - \mathbf{f}_{ext} = 0 \; , \tag{10}$$

where $\mathbf{u}$ is the displacement vector, $\dot{\mathbf{u}}$ is the velocity vector, $\ddot{\mathbf{u}}$ is the acceleration vector and $\mathbf{M}$ denotes the consistent mass matrix. The vectors $\mathbf{f}_{int}$, $\mathbf{f}_c$, and $\mathbf{f}_{ext}$ denote the internal, contact, and external forces of the discretized system. In expression (10) superimposed dots denote derivative with respect to time. The expression for $\mathbf{M}$, $\mathbf{f}_{int}$, and $\mathbf{f}_{ext}$ can be found in standard texts, see eg. [Wriggers (2008)]. The expression for the contact force $\mathbf{f}_c$ is obtained from the element contributions $\mathbf{f}_{ck}^e$ ($e = 1, \ldots, n_{sel}$ where n_{sel} is the total number of surface elements influenced by adhesion). The expression for $\mathbf{f}_{ck}^e$ acting on the n_{se} surface nodes of the current surface element Γ_k^e or the reference surface element Γ_{0k}^e is given by

$$\mathbf{f}_{ck}^e = -\int_{\Gamma_k^e} \mathbf{N}_e^T t_k da_k = -\int_{\Gamma_{0k}^e} \mathbf{N}_e^T T_k dA_k \; , \tag{11}$$

where $\mathbf{N}_e$ is given as

$$\mathbf{N}_e = [N_1\mathbf{I}, N_2\mathbf{I}, \ldots, N_{n_{se}}\mathbf{I}] \; , \tag{12}$$

which is a $[n_{dim} \times (n_{dim} + n_{se})]$ dimensional matrix formed by the n_{se} surface shape functions N_I ($I = 1, 2, \ldots, n_{se}$) of the surface element. Here, $n_{dim} \leq 3$ is the dimension of the Euclidean space occupied by the reference configuration and $\mathbf{I}$ is an identity matrix of size $n_{dim} \times n_{dim}$. In general, both $\mathbf{f}_{int}$ and $\mathbf{f}_c$ may depend on the displacement and velocity, i.e., $\mathbf{f}_{int} = \mathbf{f}_{int}(\mathbf{u}, \dot{\mathbf{u}})$, and $\mathbf{f}_c = \mathbf{f}_c(\mathbf{u}, \dot{\mathbf{u}})$. However, in the current work, we always consider $\mathbf{f}_c = \mathbf{f}_c(\mathbf{u})$. Also, it is assumed that the internal force vector $\mathbf{f}_{int} = \mathbf{f}_{int}(\mathbf{u}, \dot{\mathbf{u}})$ can be additively split into an elastic part and a viscous part that is linear in $\dot{\mathbf{u}}$ i.e.,

$$\mathbf{f}_{int}(\mathbf{u}, \dot{\mathbf{u}}) = \mathbf{f}_{el}(\mathbf{u}) + \mathbf{C}\dot{\mathbf{u}} \; , \tag{13}$$

where $\mathbf{C}$ is the damping matrix. We consider Rayleigh damping in which the damping matrix can be written as

$$\mathbf{C} = \alpha_1 \mathbf{M} + \alpha_2 \mathbf{K}_{el,0} \; , \tag{14}$$

where $\mathbf{K}_{el,0}$ denotes the constant stiffness matrix at $\mathbf{f}_{el} = \mathbf{0}$. In Eq. (14), α_1, and α_2 are mass and stiffness proportional damping constants respectively. Hence, the equation of motion given by Eq. (10) is obtained as

$$\mathbf{M}\ddot{\mathbf{u}} + \mathbf{C}\dot{\mathbf{u}} + \mathbf{f}_{el} + \mathbf{f}_c - \mathbf{f}_{ext} = 0 \; . \tag{15}$$

4

3 Time Integration Schemes

The numerical solution of Eq. (15) requires integration in time for which suitable time integration schemes are required. In the present section, we first present two collocation-based time integration schemes. The first scheme is the Newmark scheme [Newmark (1959)] which is a parameter-based scheme. The second scheme is the composite scheme proposed by Bathe and coworkers [Bathe (2007); Bathe and Baig (2005); Bathe and Noh (2012)] which belongs to the parameter-free family schemes. Then, we present the details of the composite time integration scheme proposed in this work.

3.1 Parameter-based time integration scheme: Newmark scheme [Newmark (1959)]

The standard Newmark equations are given as

$$\mathbf{u}^{n+1} = \mathbf{u}^n + \Delta t \, \dot{\mathbf{u}}^n + \frac{\Delta t^2}{2} \left[(1 - 2\beta) \, \ddot{\mathbf{u}}^n + 2\beta \, \ddot{\mathbf{u}}^{n+1} \right] , \tag{16}$$

$$\dot{\mathbf{u}}^{n+1} = \dot{\mathbf{u}}^n + \Delta t \left[(1 - \gamma) \, \ddot{\mathbf{u}}^n + \gamma \ddot{\mathbf{u}}^{n+1} \right] , \tag{17}$$

where Δt is the time step and β and γ are the Newmark parameters. The acceleration $\ddot{\mathbf{u}}^{n+1}$ is obtained by substituting for $\mathbf{u}^{n+1}$ and $\dot{\mathbf{u}}^{n+1}$ in Eq. (10). In the present work, even though we consider a nonlinear system, the values of the parameters β and γ are chosen as $1/4$ and $1/2$ which correspond to an unconditionally stable scheme for the linear system with explicitly prescribed external loads. Substitution for $\ddot{\mathbf{u}}^{n+1}$ from Eq. (16) in Eq. (10) leads to the force residual

$$\mathbf{f}_{\text{res}}^{n+1} = \mathbf{f}_{\text{el}}^{n+1} + \mathbf{f}_{\text{c}}^{n+1} - \mathbf{f}_{\text{ext}}^{n+1} + w_0 \mathbf{M} \left(\mathbf{u}^{n+1} - \mathbf{u}^n \right) - w_1 \mathbf{M} \dot{\mathbf{u}}^n - w_2 \mathbf{M} \ddot{\mathbf{u}}^n = \mathbf{0} . \tag{18}$$

Here, the constants w_0-w_2 are given by

$$w_0 = \frac{1}{\beta \Delta t^2} , \qquad w_1 = \frac{1}{\beta \Delta t} , \qquad w_2 = \frac{1}{2\beta} - 1 . \tag{19}$$

The residual given by Eq. (18) has to be solved using an iterative scheme to obtain the solution. In the present work, Newton-Rapshon (NR) scheme is chosen for which corresponding tangent matrix is given by

$$\mathbf{K}^{n+1} := \frac{\partial \mathbf{f}_{\text{res}}^{n+1}}{\partial \mathbf{u}^{n+1}} = \frac{\partial \mathbf{f}_{\text{el}}^{n+1}}{\partial \mathbf{u}^{n+1}} + \frac{\partial \mathbf{f}_{\text{c}}^{n+1}}{\partial \mathbf{u}^{n+1}} - \frac{\partial \mathbf{f}_{\text{ext}}^{n+1}}{\partial \mathbf{u}^{n+1}} + w_0 \mathbf{M} . \tag{20}$$

The tangent matrix associated with the contact contribution $\mathbf{f}_{\text{c}}^{n+1}$ is given by

$$\mathbf{K}_{\text{c}}^{n+1} := \frac{\partial \mathbf{f}_{\text{c}}^{n+1}}{\partial \mathbf{u}^{n+1}} = - \int_{\Gamma_{0k}^e} \mathbf{N}_e^T \frac{\partial T_k}{\partial x_k} \mathbf{N}_e \, \mathrm{d}A_k . \tag{21}$$

We refer to Sauer and Wriggers (2009) for detailed derivations and discussion. Once convergence is reached, velocity $\dot{\mathbf{u}}^{n+1}$, and acceleration $\ddot{\mathbf{u}}^{n+1}$ are computed using Eqs. (16) and (17).

Remarks: Taking $\gamma > 1/2$ and $\beta > \gamma/2$ in the Newmark scheme introduces so-called *algorithmic damping*. However, this also damps out the physically relevant lower modes and reduces the accuracy to first order. Temporal integration schemes have been developed with a controllable numerical dissipation for higher modes (see e.g., [Chung and Hulbert (1993); Krenk and Hogsberg (2005)]). A detailed analysis of energy conservation and dissipation in linear Newmark-type algorithms and their α modifications is discussed in Krenk (2006).

3.2 Parameter-free time integration scheme: Bathe composite scheme [Bathe (2007); Bathe and Baig (2005)]

This scheme has been proposed by Bathe and coworkers [Bathe (2007); Bathe and Baig (2005)]. The scheme combines two distinct schemes to yield a *composite scheme* for the numerical integration of nonlinear dynamical system of equations. The approach used in the scheme is to calculate the unknown displacements, velocities, and accelerations by considering the time step Δt to consist of two equal sub-steps of size $\Delta t/2$. For the first sub-step solution, the trapezoidal rule is used, and for the second sub-step solution, the 3-point backward Euler formula is used. In the first sub-step, the nonlinear dynamic equation (Eq. 10)[3] is written at time $t_{n+1/2} = t_n + \Delta t/2$. The equations of the trapezoidal rule are given as

$$\mathbf{u}^{n+\frac{1}{2}} = \mathbf{u}^n + \frac{\Delta t}{4}\left(\dot{\mathbf{u}}^n + \dot{\mathbf{u}}^{n+\frac{1}{2}}\right), \tag{22}$$

$$\dot{\mathbf{u}}^{n+\frac{1}{2}} = \dot{\mathbf{u}}^n + \frac{\Delta t}{4}\left(\ddot{\mathbf{u}}^n + \ddot{\mathbf{u}}^{n+\frac{1}{2}}\right). \tag{23}$$

Combining Eqs. (10) at $t_{n+1/2} = t_n + \Delta t/2$, (22) and (23) leads to the force residual at $t_{n+1/2}$ which is given by

$$\mathbf{f}_{\text{res}}^{n+\frac{1}{2}} = \mathbf{f}_{\text{el}}^{n+\frac{1}{2}} + \mathbf{f}_{\text{c}}^{n+\frac{1}{2}} - \mathbf{f}_{\text{ext}}^{n+\frac{1}{2}} + w_4\mathbf{M}\mathbf{u}^{n+\frac{1}{2}} - \mathbf{M}\left(w_4\mathbf{u}^n + 2w_3\dot{\mathbf{u}}^n + \ddot{\mathbf{u}}^n\right) = \mathbf{0}, \tag{24}$$

where the constants w_3 and w_4 are given by

$$w_3 = \frac{4}{\Delta t}, \qquad w_4 = \left(\frac{4}{\Delta t}\right)^2. \tag{25}$$

The tangent matrix associated with the contact contribution $\mathbf{f}_{\text{c}}^{n+\frac{1}{2}}$ required for NR iterations follows similar procedure as in Newmark scheme, see Sauer and Wriggers (2009) for details. Once NR convergence is reached, velocity $\dot{\mathbf{u}}^{n+\frac{1}{2}}$, and acceleration $\ddot{\mathbf{u}}^{n+\frac{1}{2}}$ are computed using Eqs. (22) and (23). In the second sub-step, the nonlinear dynamic equation (Eq. 10) is written at time $t_{n+1} = t_n + \Delta t$. The equations of the three-point Euler backward method are given as

$$\dot{\mathbf{u}}^{n+1} = w_5\mathbf{u}^n - w_3\mathbf{u}^{n+\frac{1}{2}} + w_6\mathbf{u}^{n+1}, \tag{26}$$

$$\ddot{\mathbf{u}}^{n+1} = w_5\dot{\mathbf{u}}^n - w_3\dot{\mathbf{u}}^{n+\frac{1}{2}} + w_6\dot{\mathbf{u}}^{n+1}, \tag{27}$$

where the constants w_5 and w_6 are given as

$$w_5 = \frac{1}{\Delta t}, \qquad w_6 = \frac{3}{\Delta t}. \tag{28}$$

Combining Eqs. (10) at $t_{n+1} = t_n + \Delta t$, (26) and (27) leads to the force residual at t_{n+1} which is given by

$$\mathbf{f}_{\text{res}}^{n+1} = \mathbf{f}_{\text{el}}^{n+1} + \mathbf{f}_{\text{c}}^{n+1} - \mathbf{f}_{\text{ext}}^{n+1} + w_4\mathbf{M}\mathbf{u}^{n+1} - \mathbf{M}\left(w_0w_3\mathbf{u}^{n+\frac{1}{2}} + w_5\mathbf{u}^n - w_0\dot{\mathbf{u}}^{n+\frac{1}{2}} + \right.$$
$$\left. w_2\dot{\mathbf{u}}^n\right) = \mathbf{0}, \tag{29}$$

where the constants w_7 and w_8 are given as

$$w_7 = \left(\frac{3}{\Delta t}\right)^2, \qquad w_8 = \frac{3}{\Delta t^2}. \tag{30}$$

The tangent matrix associated with the contact contributions $\mathbf{f}_{\text{c}}^{n+1}$ follows similar procedure as in Newmark scheme, see Sauer and Wriggers (2009) for details. After convergence is reached velocity $\dot{\mathbf{u}}^{n+1}$, and acceleration $\ddot{\mathbf{u}}^{n+1}$ are computed using Eqs. (26) and (27).

---

[3]In case of damping, we use Eq. (15) instead of Eq. (10).

Remarks: This scheme, unlike Newmark scheme, has no parameter to choose or adjust. The method is shown to be second order accurate and remains stable for large deformation and long time response. Also, it has been shown recently, see [Noh et al. (2013)], to dissipate spurious higher modes which arise because of the spatial discretization. A time step value below a certain threshold leads to no dissipation.

3.3 Proposal of a new composite time integration scheme

Next, we present a new composite time integration scheme. The system of second-order ordinary differential equations given by Eq. (15) are integrated over the time interval $\mathcal{T} \in [t_n, t_{n+1}]$ to give the residual momentum vector at time t_{n+1} as

$$\mathbf{p}_{\text{res}}^{n+1}\left(\mathbf{x}^{n+1}\right) = \mathbf{M}\left(\dot{\mathbf{u}}^{n+1} - \dot{\mathbf{u}}^n\right) + \mathbf{C}\left(\mathbf{u}_{n+1} - \mathbf{u}_n\right) + \int_{t_n}^{t_{n+1}} \left(\mathbf{f}_{\text{el}} + \mathbf{f}_{\text{c}} - \mathbf{f}_{\text{ext}}\right) \mathrm{d}t = \mathbf{0} . \tag{31}$$

The time integral corresponding to contact force vector in Eq. (31) can be computed using standard Gaussian quadrature in time or by employing a nonstandard quadrature rule like the discrete gradient method, see for e.g. Gautam and Sauer (2013). However, as mentioned in section 1, schemes based on discrete gradient approach are restricted in application because: (a) they are specific to material properties through strain energy density function, and (b) the computation of the discrete gradient itself, specially for the bulk, may become computational expensive. In the present work, we propose to integrate the integrals in Eq. (31) separately. First, we propose to integrate the internal force vector using the trapezoidal rule. Second, we observe that due to the highly nonlinear nature of the interaction potential, see Eq.(8), an accurate computation of time integral corresponding to contact force in Eq. (31) is important. Hence, it is integrated using Gaussian quadrature with large number of Gauss points. Also, the Newmark scheme is combined with Eq. (31). This leads to a new composite time integration scheme. Substituting for $\dot{\mathbf{u}}^{n+1}$ using Eqs. (16) and (17) in Eq (31), we obtain

$$\mathbf{p}_{\text{res}}^{n+1}\left(\mathbf{x}^{n+1}\right) = w_9\mathbf{M}\left(\mathbf{u}^{n+1} - \mathbf{u}^n\right) - w_{10}\mathbf{M}\dot{\mathbf{u}}^n + w_{11}\mathbf{M}\ddot{\mathbf{u}}^n + \mathbf{C}\left(\mathbf{u}_{n+1} - \mathbf{u}_n\right)$$
$$+ \int_{t_n}^{t_{n+1}} \left(\mathbf{f}_{\text{el}} + \mathbf{f}_{\text{c}} - \mathbf{f}_{\text{ext}}\right) \mathrm{d}t = \mathbf{0} , \tag{32}$$

where the constants w_9, w_{10}, and w_{11} are given by

$$w_9 = \frac{\gamma}{\beta \Delta t} , \qquad w_{10} = \frac{\gamma}{\beta} , \qquad w_{11} = \Delta t \left(1 - \frac{\gamma}{2\beta}\right) . \tag{33}$$

Now, as proposed, the integral corresponding to the internal force is replaced using the trapezoidal rule. Hence,

$$\int_{t_n}^{t_{n+1}} \mathbf{f}_{\text{el}} \, \mathrm{d}t = \frac{\Delta t}{2} \left(\mathbf{f}_{\text{el}}^{n+1} + \mathbf{f}_{\text{el}}^n\right) . \tag{34}$$

Finally, the tangent matrix needed for NR iterations is obtained as

$$\mathbf{L}^{n+1} := \frac{\partial \mathbf{p}_{\text{res}}^{n+1}}{\partial \mathbf{x}^{n+1}} = w_9 \mathbf{M} + \mathbf{C} + \frac{\Delta t}{2} \left(\frac{\partial \mathbf{f}_{\text{el}}^{n+1}}{\partial \mathbf{x}^{n+1}}\right) + \frac{\partial}{\partial \mathbf{x}^{n+1}} \left[\int_{t_n}^{t_{n+1}} \left(\mathbf{f}_{\text{c}} - \mathbf{f}_{\text{ext}}\right) \mathrm{d}t\right] . \tag{35}$$

Here, the integral for the internal forces is replaced by Eq. (34). In the present work, the number of Gauss points for integration in time for the contact force and external force components in Eq. (31) is taken to be 5.

4 Numerical Examples

In the present section, first, the performance of the time integration schemes outlined in section 3 is discussed using two simple problems i.e., interaction of a deformable ball with a rigid surface and peeling of a deformable strip from a rigid substrate. Then, the performance of the schemes is discussed through dynamic peeling simulation a gecko spatula from a rigid substrate. In the present work, the material is modeled as an isotropic, nonlinear elastic Neo-Hooke material with Young's modulus E and the Poisson's ratio ν are taken as 2 GPa and 0.2 respectively. The density is taken as 1000 kg/m^3. The Neo-Hookean material model given by Zienkiewicz and Taylor (2005)

$$W = \frac{\mu}{2}(\mathrm{tr}B - 3) - \mu \ln J + \frac{\Lambda}{2}(\ln J)^2 \tag{36}$$

has been considered. Here, B is the left Cauchy-Green tensor and $J = \sqrt{\det B}$. In the above expression, μ and Λ are the Lamé constants.

In the present work, a normalized form of Eq. (7) is used. For normalization of Eq. (7), we first define

$$\bar{T}_k = \frac{T_k}{E_0}, \qquad \bar{r}_s = \frac{L_0}{r_s}, \tag{37}$$

where E_0 and L_0 are the characteristic energy density (or stiffness) and length scale of the problem respectively. The normalized equation corresponding to Eq. (7) is written using the normalization procedure discussed in Sauer and Wriggers (2009), which leads to

$$\bar{T}_k = \left[\frac{c_1}{\bar{r}_s^9} - \frac{c_2}{\bar{r}_s^3}\right] n_{\mathrm{p}} = \bar{T}_k n_{\mathrm{p}}, \tag{38}$$

where the constants c_1 and c_2 are given as

$$c_1 = \frac{\pi}{45 \gamma_W \gamma_L^9}, \qquad c_2 = \frac{\pi}{3 \gamma_W \gamma_L^3}. \tag{39}$$

The parameters $\gamma_L = L_0/r_0$ and $\gamma_W = E_0/W_0$, where $W_0 = A_H/2\pi^2 r_0^3$, characterize the scale and strength of adhesion. We refer to Sauer and Li (2008) for detailed discussion on γ_L and γ_W. In the current work, the value of γ_L and γ_W are chosen as 2.5 and 25 respectively which correspond to the values found in gecko adhesion [Sauer and Holl (2013)].

4.1 Interaction of a deformable ball with a rigid surface

First, the interaction of a deformable ball with a rigid surface is considered, see Figure 1. This example has also been discussed in detail in Gautam and Sauer (2013). The diameter of the ball is taken as $D_0 = 10\,L_0$. Material damping is not considered. The ball is assumed to be released from rest. The initial separation between the ball's center and the rigid surface is taken as $r_{\mathrm{initial}} = 7L_0 + r_{\mathrm{eq}}$ where r_{eq} is the equilibrium distance corresponding to the interaction potential Φ_ℓ. The finite element mesh consists of 48 four noded quadrilateral elements. The time step for the analysis is taken as 0.001 T_0 where T_0 is the characteristic time of the problem. No adaptive time stepping is considered. In the present example, all the cases were run on the same machine for better comparison of the schemes.

Next, the variation of error in energy, ΔE, and logarithmic norm of total angular momentum $\mathbf{G}_{n+1}$ with time is shown in Figures (2(a)) and (2(b)). The error in energy ΔE is defined as

$$\Delta E := \log_{10}\left[\frac{E_n - E_0}{E_0}\right], \tag{40}$$
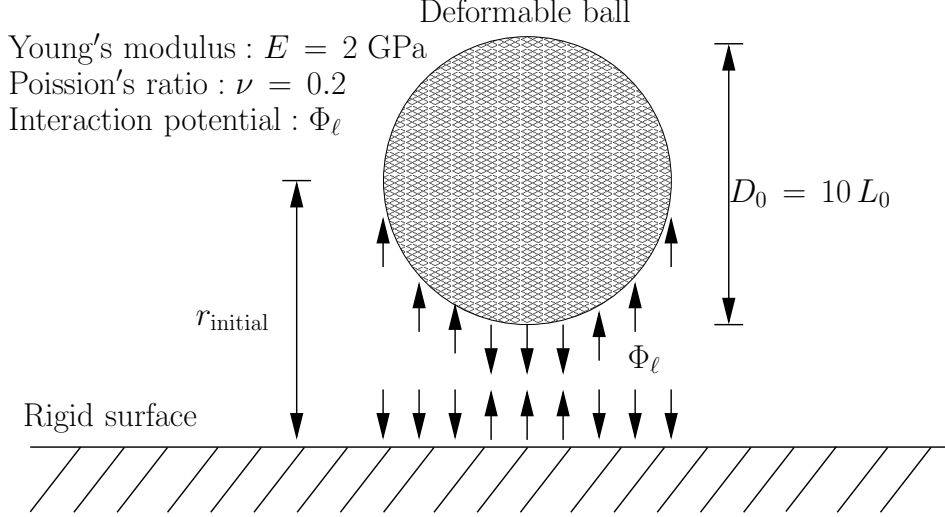
Figure 1: Initial configuration of a deformable ball interacting with a rigid surface. The diameter of the ball is taken as $D_0 = 10L_0$, $r_{\text{initial}} = 7L_0 + r_{\text{eq}}$. Here, r_{eq} is the equilibrium distance corresponding to the interaction potential Φ_ℓ. The ball is at rest at $t = 0$.

where E_0 and E_n are the energies at the start and at time $t = t_n$ respectively. The total angular momentum, $\mathbf{G}_{n+1}$, about the origin at time t_{n+1} is expressed as

$$\mathbf{G}_{n+1} = \sum_{J=1}^{n_{\text{node}}} \mathbf{x}_J^{n+1} \times \mathbf{p}_J^{n+1} , \tag{41}$$

where, $\mathbf{x}_J^{n+1}$ and $\mathbf{p}_J^{n+1}$ are the position vector and total linear momentum of node J respectively. The results of the scheme proposed by Gautam and Sauer (2013) are also included. It can be seen that the Newmark scheme diverges after $t \approx 2.5T_0$. The error of the scheme proposed by Gautam and Sauer (2013) is the lowest followed by the scheme proposed in the present work. However, the accuracy of the proposed scheme is still two order of magnitude higher than other collocation-based schemes. The variation of norm of total angular momentum, $\|\mathbf{G}_{n+1}\|$, with time shows that the Bathe composite scheme and the proposed scheme perform equally well. However, the accuracy of the scheme proposed in Gautam and Sauer (2013) is at-least 5 order of magnitude higher than the proposed scheme. However, the momentum conservation properties of proposed scheme is better than Gautam and Sauer (2013). The total computation time and computational time per increment is shown in Table 1. The computational time per increment using Newmark scheme is 0.6150 seconds per increment where as it is 0.706 seconds for the proposed scheme. The Bathe composite scheme requires 1.201 seconds per increment. The reason is that in the Bathe composite scheme each increment is composed of two equal substeps leading to more computational time. The scheme proposed Gautam and Sauer (2013) takes 8.560 seconds per increment on the same machine.

Table 1: Computational time required for different schemes.

S. No.	Numerical scheme	Total time (sec)	Time per increment (sec)
1.	Newmark (1959)	3784 (until 2.65 T_0)	0.615
2.	Bathe (2007)	12007	1.201
3.	Proposed scheme	7054	0.706
4.	Gautam and Sauer (2013)	42810	8.560

9

(a) Error in energy ΔE

(b) Norm of angular momentum $\log_{10}(\|\mathbf{G}_{n+1}\|)$
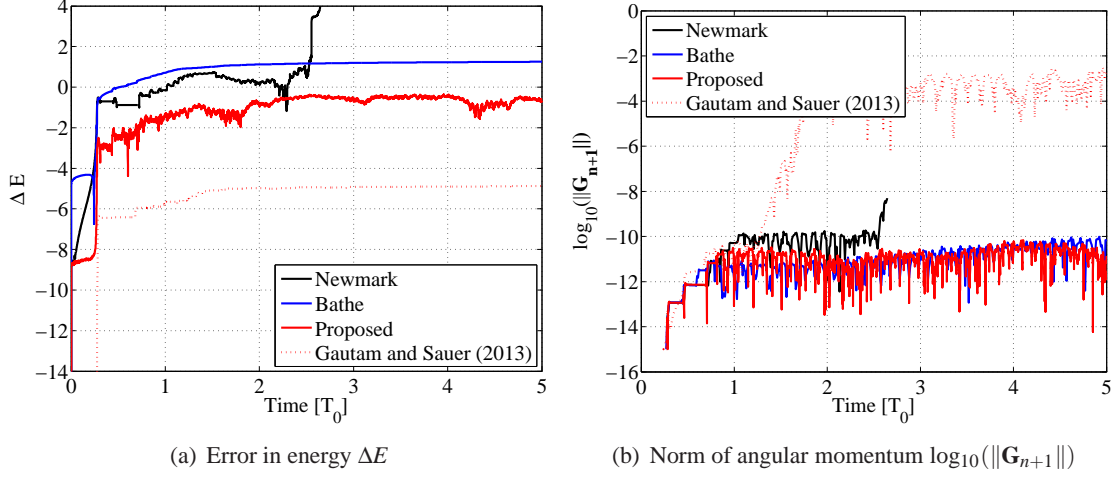
Figure 2: Variation of error in energy ΔE and norm of angular momentum $\log_{10}(\|\mathbf{G}_{n+1}\|)$ over time for various schemes. In (a), it can be seen that the Newmark scheme diverges at $t \approx 2.5\,T_0$. The adhesion parameters are: $\gamma_L = 2.5$, $\gamma_W = 25$. The scheme proposed in Gautam and Sauer (2013) gives better energy conservation.

4.2 Peeling of a deformable strip from a rigid substrate

Next, peeling of a deformable strip from a rigid substrate is simulated. Figure (3) shows the initial configuration. The geometric and material data are taken from Sauer (2011). The strip is considered to have a length $L = 200L_0$ and height $h = 10L_0$. Plain strain situation is considered. The strip, initially at rest, is peeled off the substrate by applying a time varying displacement $\bar{u} = \bar{u}(t)$ on the right side edge such that the velocity of pull is $\dot{\bar{u}} = 1$ m/s. The displacement is applied with initial ramp-up to avoid initial shock to the strip. The displacement is applied until the Y coordinate of the point P (see Fig. 3) is less than $10L_0$.
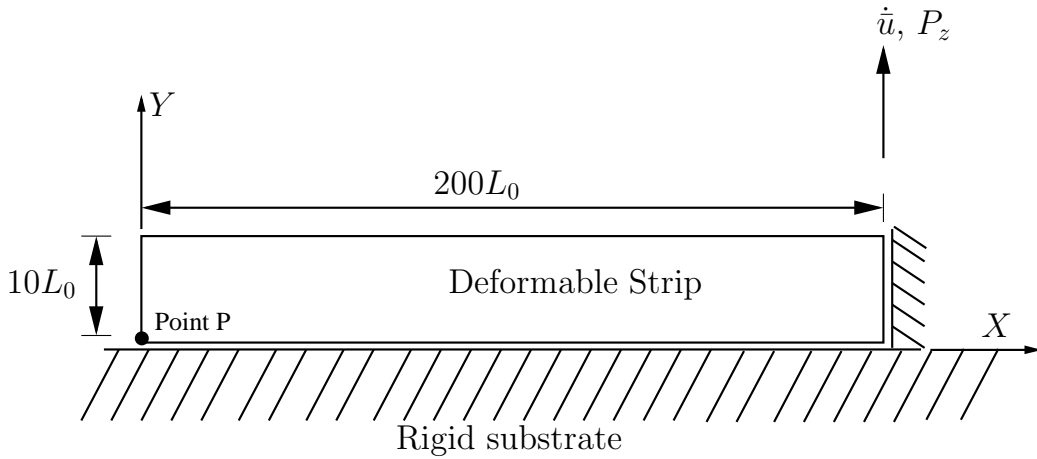
Figure 3: Initial configuration of a deformable strip adhering to a rigid substrate. The strip is pulled at $\bar{u}(t)$ at the right edge, i.e., at $X = 200L_0$ such that $\dot{\bar{u}} = 1$ m/s. At $X = 200L_0$, the strip is constrained in X direction. P_z is the unknown reaction force corresponding to $\bar{u}$.

The interaction of the strip and the rigid substrate is assumed to be governed by the interaction potential Φ_ℓ given in Eq. (8). Sixteen elements are chosen over the strip height h. The aspect ratio is kept at one. Adhesive contact is considered along the 75% of the bottom surface i.e., from $X = 0$ to $X = 150L_0$.

10

Remark: As noted in Sauer (2011) linear approximation of the displacement i.e., Q1C1 contact finite element, at the contact interface can lead to unphysical oscillations. These oscillations can be reduced using enriched contact finite elements, for e.g. Q1C2 and, Q1C4, at the contact interface[4]. Enriched contact finite elements Q1C2 and Q1C4 correspond to quadratic and fourth order approximation of displacement at the contact interface. The advantages of using Q1C2 and Q1C4 elements is discussed in section 4.2.3.

4.2.1 Description of the peeling process

First, the peeling process is explained. The results are presented for the time step $\Delta t = 0.01 T_0$. Enriched contact finite element Q1C4 is employed at the contact interface. The configurations at different time instances are shown in Fig. (4). The peeling starts at $T = 40 T_0$ (Fig. 4(c)). The configuration at $T = 130 T_0$ (Fig. 4(j)) shows the strip just before it completely peels off from the substrate. Various intermediate configurations at different time instances are also shown. The corresponding pull-off force with time is shown in Fig. (5) for the three schemes. The markers 'A-J' on Fig. (5) correspond to different configurations shown in Fig. (4). The phase until point 'C' is when the strip stretches without peeling. The maximum peel-off force is reached when the peel-off starts. The phase from 'C' to 'I' correspond to stable peeling. After this, the remaining part of the strip snaps off from the substrate leading to fluctuation in peel-off force as marked in point 'J'. The simulation is stopped when the strip has completely peeled-off from the surface. It can be seen that all the schemes have similar response.

The variation of the resultant velocity of point P (see Fig. 3) for different schemes is shown in Fig. (6(a)). It can be seen that all the schemes give similar response. The oscillations in the response (Fig. 6(b)) are because of numerical artifacts which arise due to spatial discretization at the contact interface. Section 4.2.3 further discusses this behavior.

In the further text, the results of this sections are treated as exact results since no closed form solution is available. In the figures that follow, the text *'Exact'* is used. Also, in the results that follow the variation of peel-off force with applied displacement for different cases is only shown at start of the peeling. Similarly, the variation of resultant velocity with time of point P for different cases is shown only at the end of peeling.

4.2.2 Response of the schemes

The response of the three schemes for different time steps i.e., $\Delta t = 1 T_0$, $0.1 T_0$, and $0.05 T_0$ is presented. Figure (7) shows the pull-off force with time at the start of the peeling. Linear displacement interpolation, i.e. Q1C1 contact element, is used at the contact interface. The exact result is also included. It can be seen that as the time step is decreased oscillations appear in the response which is because the spatial discretization at the contact interface is unable to accurately resolve the contact forces (Eq. 9). It is later shown in section 4.2.3 that the enriched contact elements proposed by Sauer (2011) can resolve the contact forces more accurately. All the schemes, however, give similar response for all the time steps. The variation of resultant velocity of point P (see Fig. 3) with time at the end of peeling is shown in Fig. (8). It can be seen from Fig. (8(a)) that the proposed and the Bathe's composite schemes do not have the oscillatory behavior of the Newmark scheme. Unphysical oscillations are observed for all the schemes with reducing the time step i.e. $\Delta t = 0.1 T_0$ and $0.05 T_0$. However, the oscillations are about the exact value.

---

[4]See Sauer (2011) for detailed discussion on the performance of enriched contact finite elements applied to static peeling problems.

(a) $T = 10T_0$: A
(b) $T = 30T_0$: B
(c) $T = 40T_0$: C
(d) $T = 50T_0$: D
(e) $T = 60T_0$: E
(f) $T = 70T_0$: F
(g) $T = 90T_0$: G
(h) $T = 110T_0$: H
(i) $T = 120T_0$: I
(j) $T = 130T_0$: J
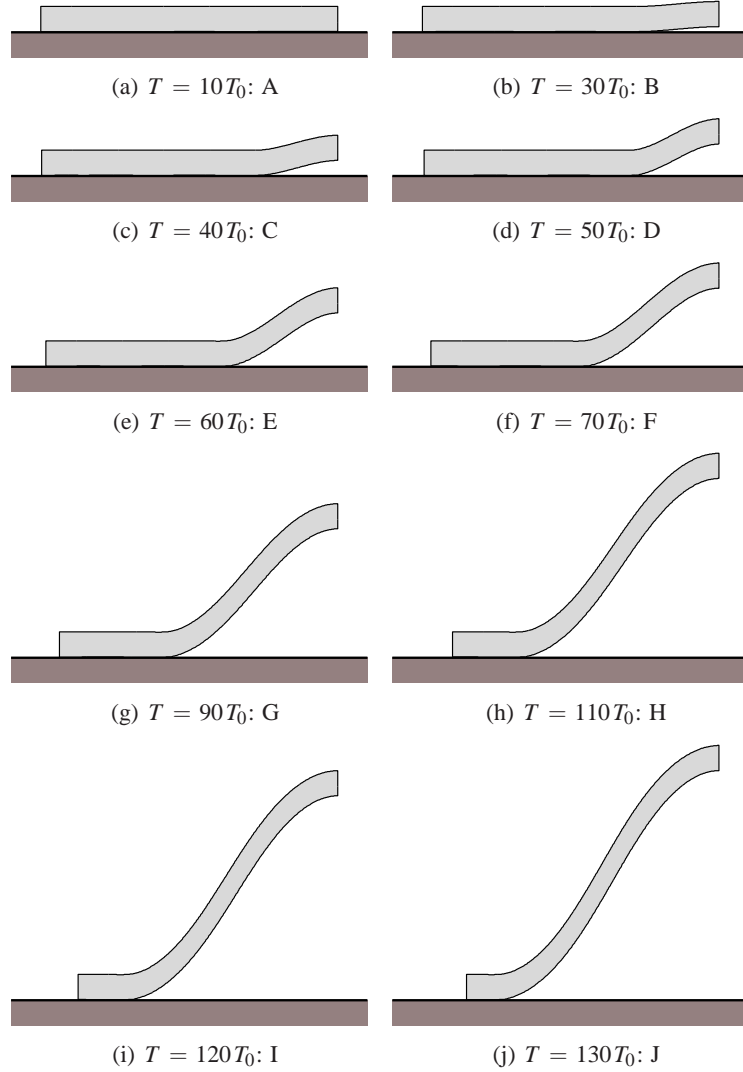
Figure 4: Deformed configurations at various time instances of a deformable strip peeling from a rigid substrate. The interaction between the strip and rigid substrate is assumed frictionless.

4.2.3 Effect of enriched contact finite elements

The oscillations in the response observed in previous section using linear interpolation at the contact interface with decreasing the time step are unphysical. As mentioned earlier, this is because the linear displacement interpolation at the contact interface is unable to accurately resolve the contact forces given by Eq. (9). To alleviate the problem enriched contact finite elements have been proposed recently by Sauer (2011). In this work, however, the results are presented for dynamic peeling. Figure (9) shows the details of the pull-off force with time using the proposed scheme for three different time steps. It can be seen clearly, (see Fig. (9(d))), that the unphysical oscillatory response for smaller time steps is reduced when using enriched contact finite elements at the contact interface.

Figure (10) shows the plot of resultant velocity of point P (see Fig. 3) with time for three different time steps using the proposed scheme. It can be seen that for all the time steps linear interpolation leads to oscillatory response which are reduced when enriched contact finite elements are used. The response using the Q1C4 element for all the time steps is closest to exact result.
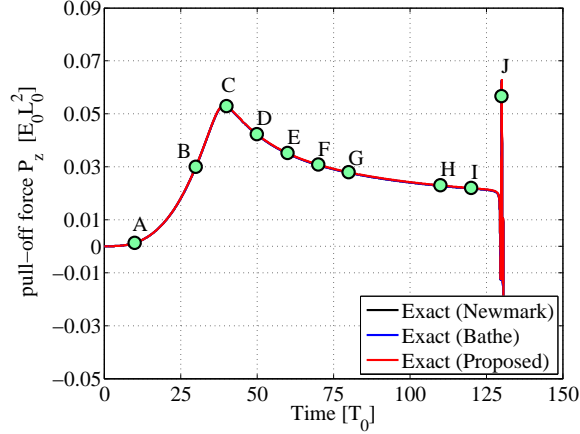
Figure 5: Variation of pull-off force with time using Q1C4 enriched contact finite element. The time step used is $\Delta t = 0.01\, T_0$. It is seen that all schemes give nearly similar responses. The markers 'A'-'J' on the curve show the pull-off force corresponding to the configurations in Fig. (4).

(a) Complete response

(b) At the end of peeling
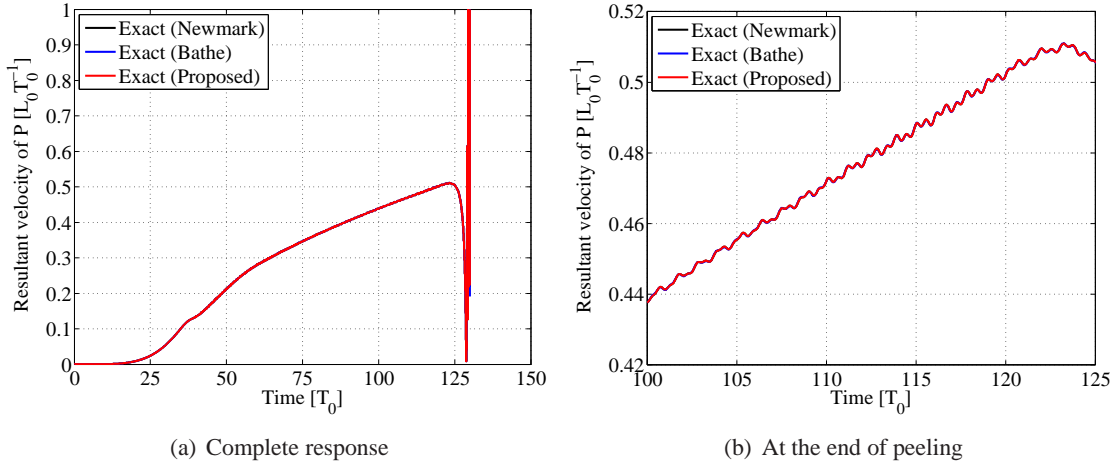
Figure 6: Variation of resultant velocity of point P with time using different schemes and Q1C4 enriched finite element at the contact interface. The time step used is $\Delta t = 0.01\, T_0$. All schemes gives similar response. The oscillations in the response shown in (b) are artifacts of the spatial discretization at the contact interface.

4.2.4   Comment on computational time

We conclude this section by presenting the computational time required for various schemes at different time steps using three enriched contact finite elements at the contact interface, see Fig. (11). All the results have been obtained by running the various cases on the same machine. It is clearly seen that the proposed scheme adds very little to the computational cost with respect to Newmark scheme even when additional degree of freedoms are added by using enriched contact finite elements. Also, it can be seen that the computational time of the proposed scheme is considerably lower as compared to Bathe composite scheme for same contact interface discretization. This is since the Bathe composite scheme divides each time step into two equal substeps which leads to higher computational cost. The saving in computational time is particulary beneficial for systems with large degree of freedom systems specially three dimensional cases as discussed next.

13

(a) $\Delta t = 1\,T_0$

(b) $\Delta t = 0.1\,T_0$

(c) $\Delta t = 0.05\,T_0$
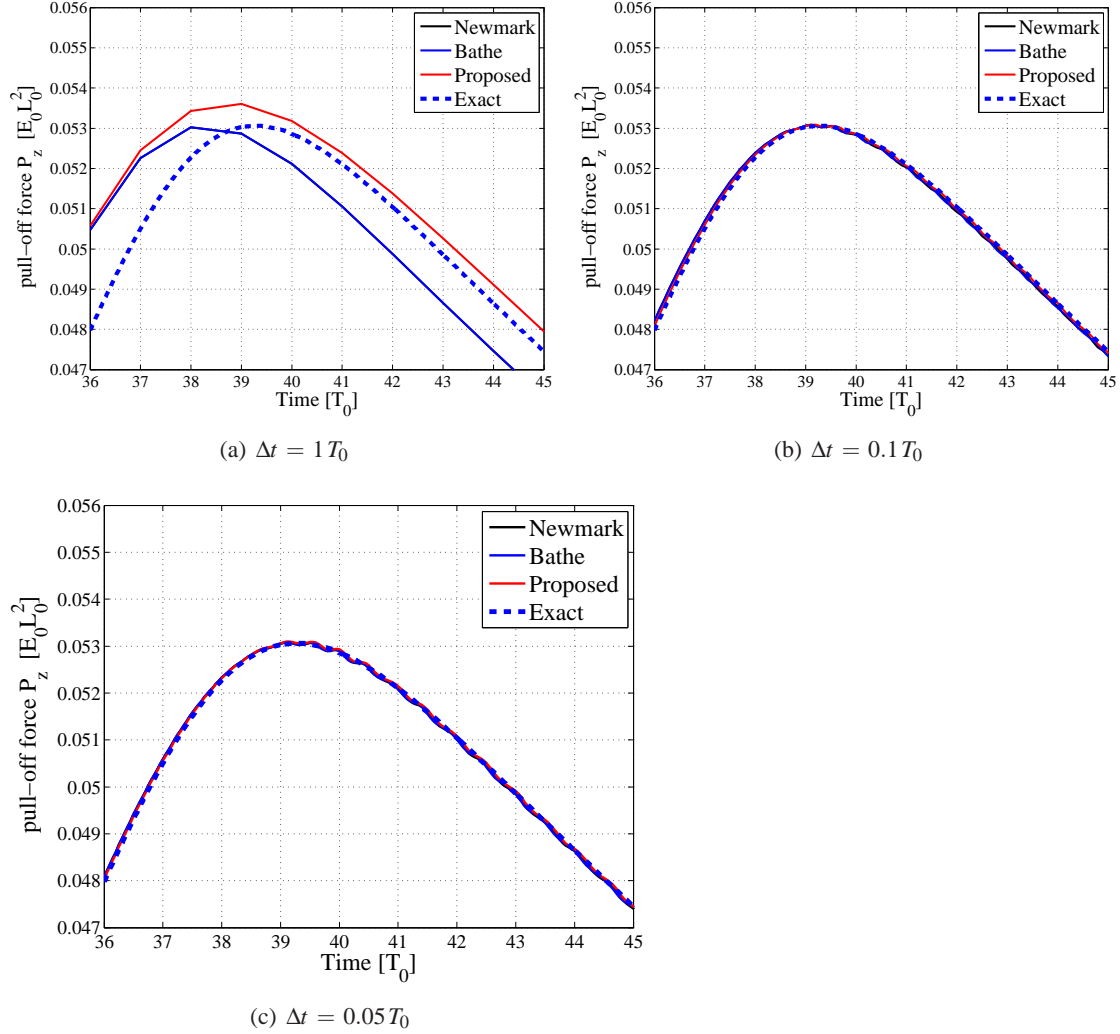
Figure 7: Variation of pull-off force with time using the Q1C1 element. The exact results are also included. The oscillations in the response are because of numerical artifacts which arise due to spatial discretization at the contact interface.

4.3 Peeling of a gecko spatula

Finally, the dynamic pull-off behavior of the gecko spatula is analyzed. First, the Gecko adhesive system is presented. Then, we discuss the procedure for selecting the values of the damping parameters: α_1 and α_2, required for Rayleigh damping, see Eq. (14). Finally, some representative numerical results are shown using the three different time integration schemes considered in the present work.

4.3.1 Gecko adhesive system

One of the remarkable qualities of geckos is their ability to climb vertical and overhead surfaces and move around with comparatively high speeds when required. This remarkable quality has led to significant research in understanding the underlying mechanisms of *gecko adhesion*. Figure (12) shows the gecko adhesive system. In the figure, 'A' shows a gecko, the size of which is approximately 10 cm while 'B' shows the toes of the gecko foot with hundreds of parallel lines of hair-like structures called the *lamella* of approximately 1-2 mm in size. Further zooming in ('C' in the figure) shows hundreds of micrometer size ($\sim 100\,\mu$m) fine hairs called the *seta*. An individual seta is shown in 'D' which branches

(a) $\Delta t = 1\,T_0$

(b) $\Delta t = 0.1\,T_0$

(c) $\Delta t = 0.05\,T_0$
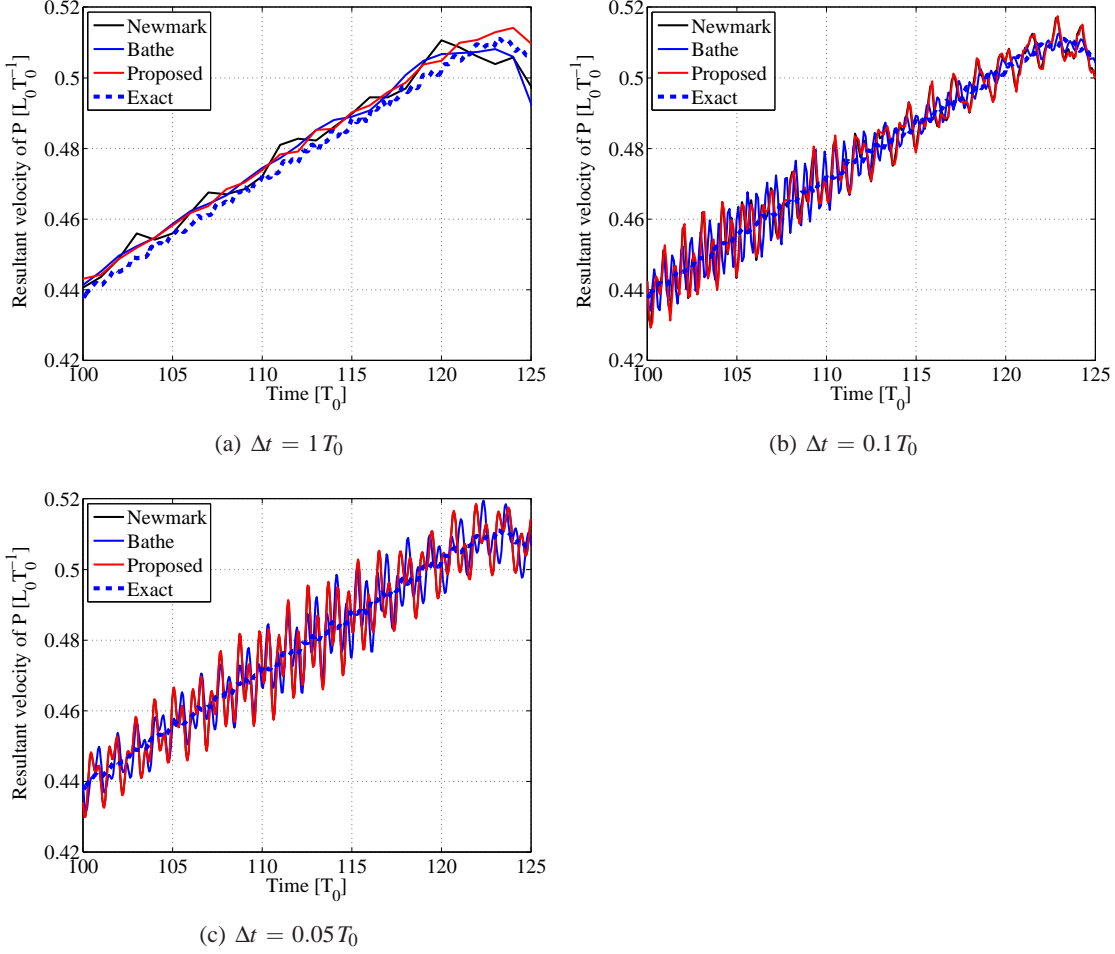
Figure 8: Variation of resultant velocity of point P with time using different time steps and Q1C1 enriched finite element at the contact interface. All schemes gives similar responses. Smaller time steps lead to unphysical oscillations in the response.

into hundreds of finer hair-like structures (further zoomed in inset 'E') called spatulae (see Fig. 13 for the microscopic images of an individual spatula). These spatulae transfer the adhesive and frictional forces between the gecko and the substrate through large mechanical deformations and rotations. The spatulae form an elemental part in the understanding of gecko adhesion. Thus, it is clear that the gecko adhesive system is a complex multi-level hierarchial structure. Understanding the adhesive mechanism of gecko, thus, requires first understanding the peeling behavior of an individual spatula.

4.3.2 Details of applied load and finite element mesh of a gecko spatula

Before we present the numerical analysis of dynamic peeling of a gecko spatula, we present the loading condition and finite element mesh considered for a single gecko spatula. The detailed geometry model of the spatula has been presented and discussed in detail in references [Sauer (2009); Sauer and Holl (2013)]. Figure (14) shows the the initial configuration of the spatula. The interaction of the gecko spatula and the rigid substrate is assumed to be governed by the interaction potential Φ_ℓ given in Eq. (8). A vertical displacement $\bar{u} = \bar{u}(t)$ is applied to the spatula shaft such that a constant pull-off velocity $\dot{\bar{u}} = 1$ m/s is achieved. The final pull-off velocity is reached after an initial ramp-up so as to avoid sudden loading of the spatula. The finite element mesh of the gecko spatula consists of 114,414 elements and 363,144 degrees of freedom. A 3D enriched contact finite element, see reference [Sauer (2011)], is

15
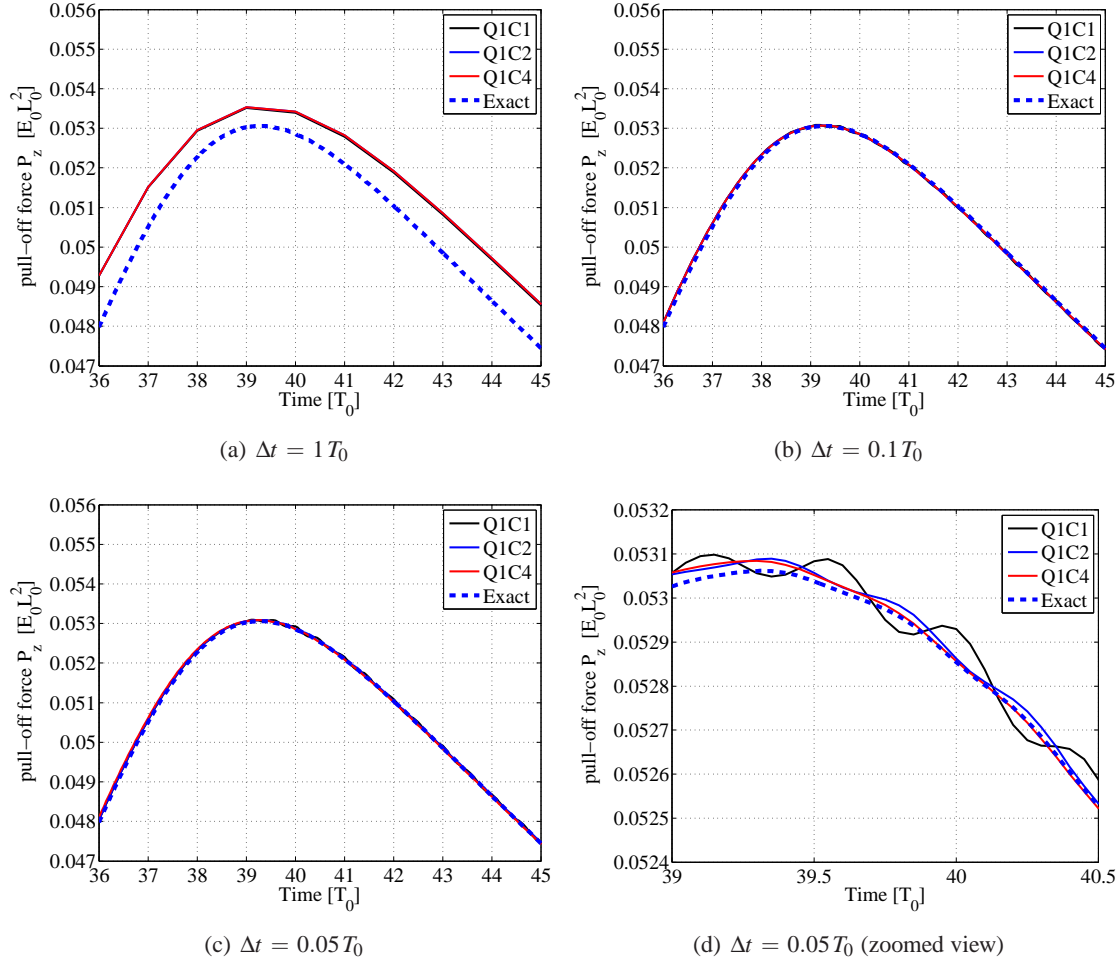
Figure 9: Variation of pull-off force with time using the proposed composite scheme. The exact results are also included. The oscillations, as seen in Fig. (9(d)), in the response are because of numerical artifacts which arise due to spatial discretization at the contact interface.

employed at the contact interface. Also, to avoid using very small time steps numerical damping is considered. The procedure for choosing the damping coefficients, based on numerical experiments, is discussed next.

4.3.3 Choice of damping parameters α_1 and α_2

In the present work, we focus only on stiffness proportional damping such that $\alpha_1 = 0$. A free vibration analysis of the gecko spatula is carried out using the Newmark scheme and the Bathe composite scheme for selecting an appropriate value for α_2. Figure (15) shows the variation of X and Z coordinates of a point P (see Fig. 14) on the spatula pad for the case with Newmark scheme for different value of α_2. It can be seen that some values lead to over damped response while other values lead to under damped response. Also, it can be seen that for the case with no damping the Newmark scheme fails after $t = 180T_0$. For the results that follow, $\alpha_2 = 0.004/ns$ is chosen for simulations. Figure (16) shows the comparison of Newmark and Bathe composite scheme. It can also be observed that the Bathe composite scheme is long time stable. Both the schemes give similar response when damping is considered.

(a) $\Delta t = 1\,T_0$

(b) $\Delta t = 0.1\,T_0$

(c) $\Delta t = 0.05\,T_0$
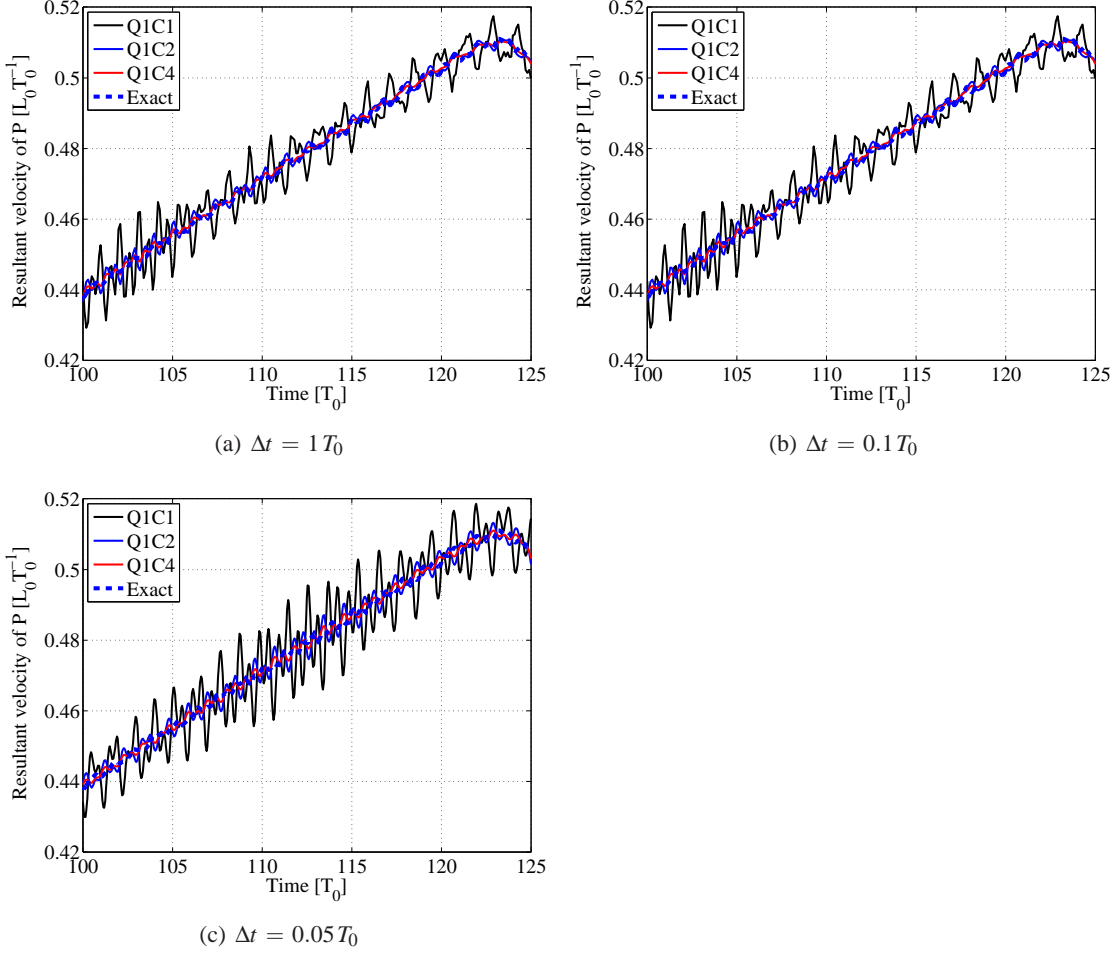
Figure 10: Variation of resultant velocity of point P with time using the proposed scheme for different time steps and different enriched finite element. It can be seen that use of enriched contact elements leads to reduction in oscillatory response.

4.3.4 Numerical analysis of gecko spatula peeling

Here, we present results for the dynamic peeling of gecko spatula from a rigid substrate. Figure (17) shows the spatula configuration at different time instances. The Bathe composite scheme is employed for time integration. The peeling front can be seen moving along the spatula surface.

Next, the performance of proposed scheme is compared with Newmark and Bathe composite scheme. The variation of pull-off force with time for the three schemes is shown in Fig. (18). The response of the Newmark scheme shows spurious oscillations (Fig. 18(b)) while the Bathe composite scheme as well as the proposed scheme give a smoother response. Also, it can be seen that the Newmark scheme diverges. After the spatula has completely peeled-off the vibrations of the spatula are quickly damped when using the Bathe composite scheme as the kinetic energy quickly reduces to zero, see Fig. (19). However, for the case when the proposed scheme is used, the spatula oscillates for longer. This is because the kinetic energy decreases slowly, see Fig. (19). However, no reference results are available to ascertain the accuracy of the schemes for the post peel-off behavior.

The maximum spatula pull-off force, which is reached prior to complete peel off, is ~ 8 nN. This value is in agreement with measured spatula pull-off loads reported in the literature, e.g. [Huber et al. (2005); Sun et al. (2005)]. However, the experimental force displacement results reported in Autumn et al. (2000) have been performed on a seta where the seta is pulled both parallel and perpendicular to the sur-

17
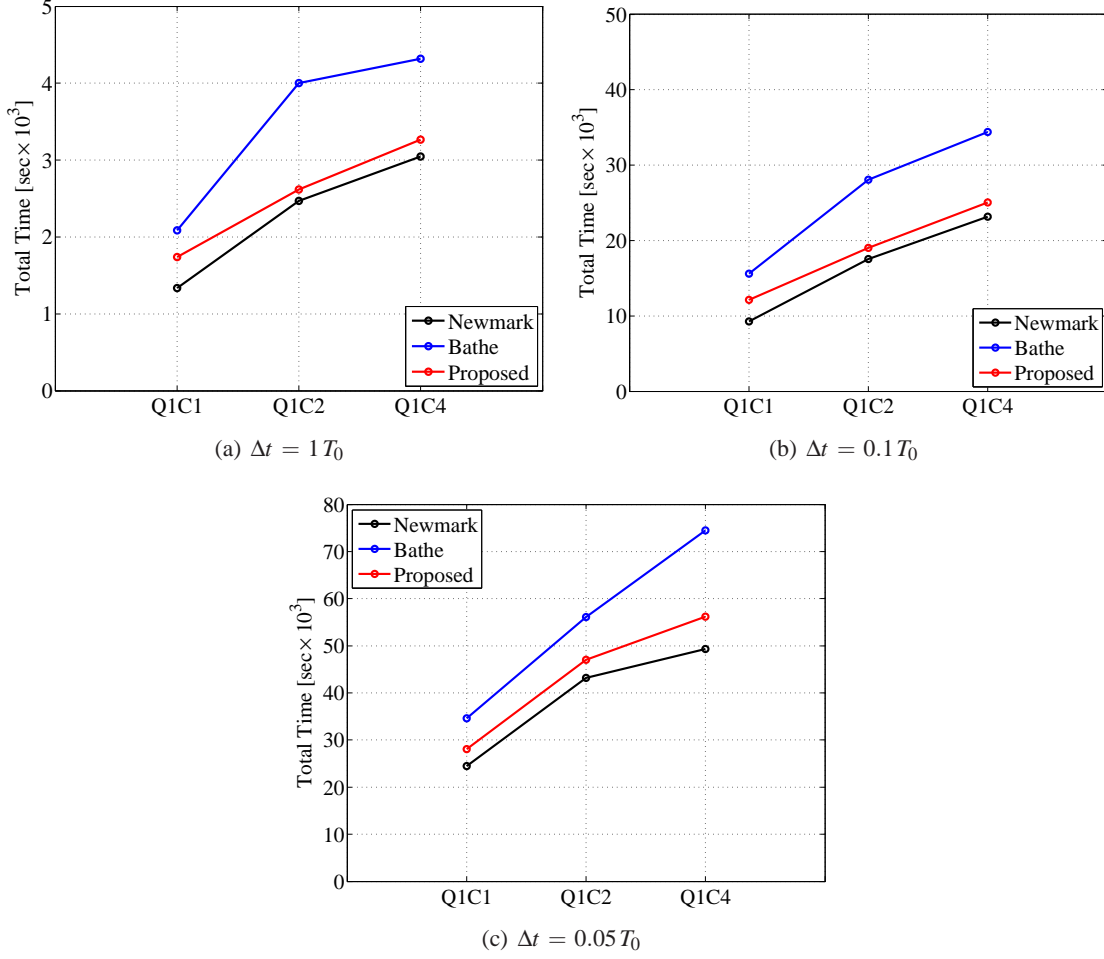
Figure 11: Computational time required for various schemes at different time steps using three enriched contact finite elements at the contact interface.

face. A single seta consists of around 100-1000 spatulae. Hence, the results reported by Autumn et al. (2000) are combined results of all the spatulae and not a single spatula. Hence, for around 1000 spatulae, an estimate based on results of single spatula of current work results in maximum pull off force of 8 μN. This is in range of the perpendicular pull-off force reported in Autumn et al. (2000) (see Fig. 4 in the reference). However, since in the present work the results reported are based on a single spatula, to simulate the experimental data reported by Autumn et al. (2000), a detailed simulation of peeling of seta is required. Such a study will be carried out in a future work.

Figure (20(a)) shows the computational effort i.e., computational time required per increment, for spatula peeling using different schemes. It can be seen that the proposed scheme adds very little to the overall computational effort. As seen from Fig. (20(b)), the computational effort per increment per NR iteration is higher for the proposed scheme. However, since the number of NR iterations per increment (see Fig 20(c)) is much higher for the Bathe composite scheme (due to solving the equation of motion twice in each time step), the over all computational time of the Bathe composite scheme is higher.

5 Concluding remarks

Dynamic adhesive contact simulations specially involving peeling have attracted very little attention. In the present work, a composite time integration scheme is proposed for simulation of dynamic adhesive
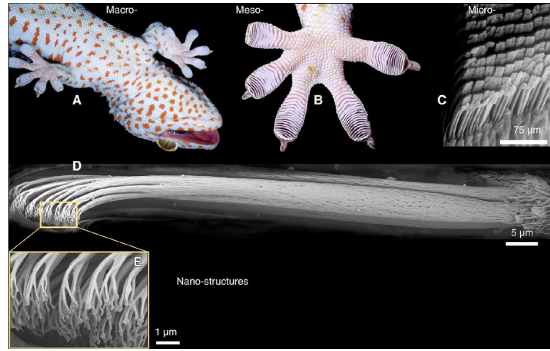
Figure 12: Gecko adhesive system. Notice the multi-level hierarchial structure of the gecko adhesive system. In the figure: 'A' shows a gecko ($\sim$ 10 cm), 'B' shows a gecko foot with hundreds of hair-like structure called the *lamellas* ($\sim$ 1-2 mm), 'C' shows the zoomed view of the gecko pad showing the *setas* ($\sim$ 100 μm), 'D' shows a single gecko *seta*, and 'E' shows zoomed view of the tip of seta showing the so-called *spatulae*. Figures have been adapted with permission from Autumn et al. (2006).

contact problems. The performance of the proposed scheme is compared with two class of collocation-based schemes: Newmark scheme which is a parameter-based scheme and Bathe composite scheme which is a parameter-free scheme. Following conclusions are drawn based on the numerical simulation of a number of example problems:

1. The Bathe composite scheme and the proposed scheme remain stable for all the cases. The Newmark scheme diverges for some cases.

2. In the first example i.e., dynamic interaction of a deformable ball with a rigid surface, it is shown that the proposed scheme leads to accuracy gains and adds very little to the overall computational effort.

3. All the schemes give similar response for the peeling of a deformable strip from a rigid substrate. However, the computational cost of the proposed scheme is smaller compared to Bathe composite scheme and only marginally higher compared to the Newmark scheme.

4. The Newmark scheme diverges in the peeling of a gecko spatula from a rigid substrate. The Bathe composite scheme and the proposed scheme are able to simulate the spatula behavior after the complete peel off. It is also shown that the computational effort required using the proposed scheme is lower.

The presented work is highly relevant to general adhesion and debonding problems. Further consideration are incorporation of friction effects and material damping.

6 Acknowledgments

References

Autumn, K., Liang, Y. A., Hsieh, S. T., Zesch, W., Chan, W. P., Kenny, T. W., Fearing, R., and Full, R. J. (2000). Adhesive force of a single gecko foot-hair. *Nature*, 405:681–684.
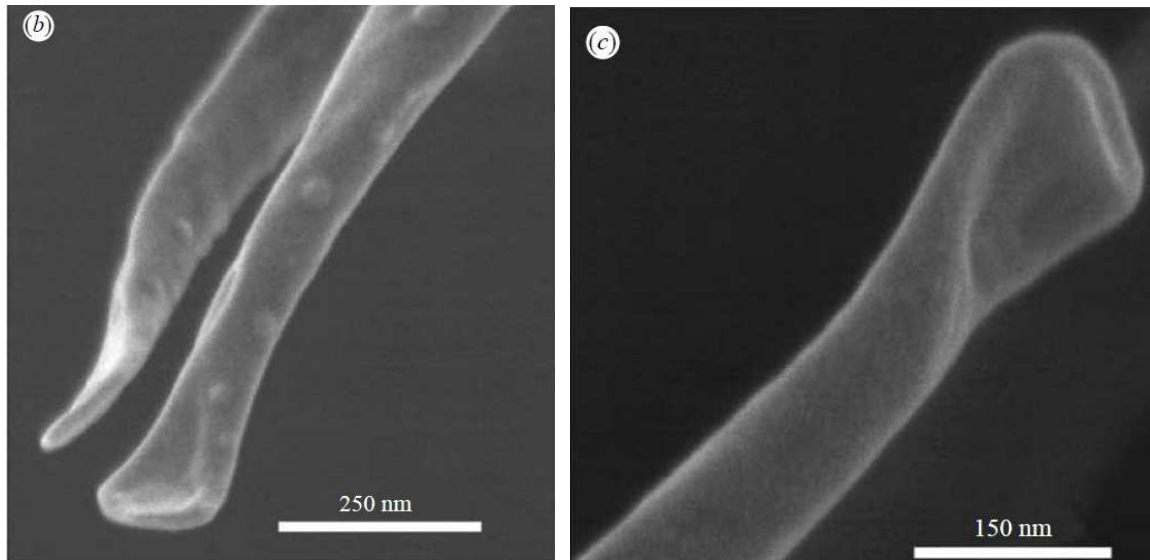
(a) Individual gecko spatula view 1   (b) Individual gecko spatula view 2

Figure 13: Microscopic images of the gecko spatula. Notice that the size of an individual spatula is around $\sim$ 150-300 nm. Figures have been adapted with permission from Rizzo et al. (2006).

Autumn, K., Majidi, C., Groff, R. E., Dittmore, A., and Fearing, R. (2006). Effective elastic modulus of isolated gecko setal arrays. *J. Exp. Biology*, 209:3558–3568.

Bathe, K. J. (2007). Conserving energy and momentum in nonlinear dynamics. *Comput. Struct.*, 85:437–445.

Bathe, K. J. and Baig, M. M. I. (2005). On a composite implicit time integration procedure for nonlinear dynamics. *Comput. Struct.*, 85:2513–2524.

Bathe, K. J. and Noh, G. (2012). Insight into an implicit time integration scheme for structural dynamics. *Comput. Struct.*, 98-99:1–6.

Betsch, P. and Steinmann, P. (2001). Conserving properties of a time FE method-part II: Time-stepping schemes for non-linear elastodynamics. *Int. J. Numer. Methods Eng.*, 50:1931–1955.

Chung, J. and Hulbert, G. M. (1993). A time integration algorithm for structural dynamics with improved numerical dissipation: the generalized-α method. *Transactions of ASME: J. Appl. Mech.*, 60(1):371–375.

Gautam, S. S. and Sauer, R. A. (2013). An energy-momentum conserving temporal discretization scheme for adhesive contact problems. *Int. J. Numer. Methods Eng.*, 93:1057–1081.

Gonzalez, O. (1996). Time integration and discrete hamiltonian systems. *J. Nonlinear Sci.*, 6:449–467.

Hesch, C. and Betsch, P. (2009). A mortar method for energy-momentum conserving schemes in frictionless dynamic contact problems. *Int. J. Numer. Methods Eng.*, 77:1468–1500.

Hesch, C. and Betsch, P. (2010). Transient three-dimensional domain decomposition problems: Frame-indifferent mortar constraints and conserving integration. *Int. J. Numer. Methods Eng.*, 82:329–358.

Huber, G., H, H. M., Spolenak, R., Mecke, K., Jacobs, K., Gorb, S. N., and Arzt, E. (2005). Evidence for capillarity contributions to gecko adhesion from single spatula nanomechanical measurements. *Proc. Natl. Acad. Sci. USA*, 45:1629316296.
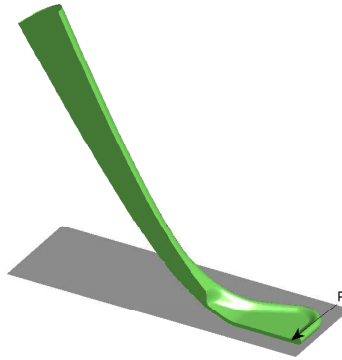
Figure 14: Initial configuration of the gecko spatula. Point P is on the bottom surface of the spatula pad.

(a) Variation of X coordinate of point P with time

(b) Variation of Z coordinate of point P with time
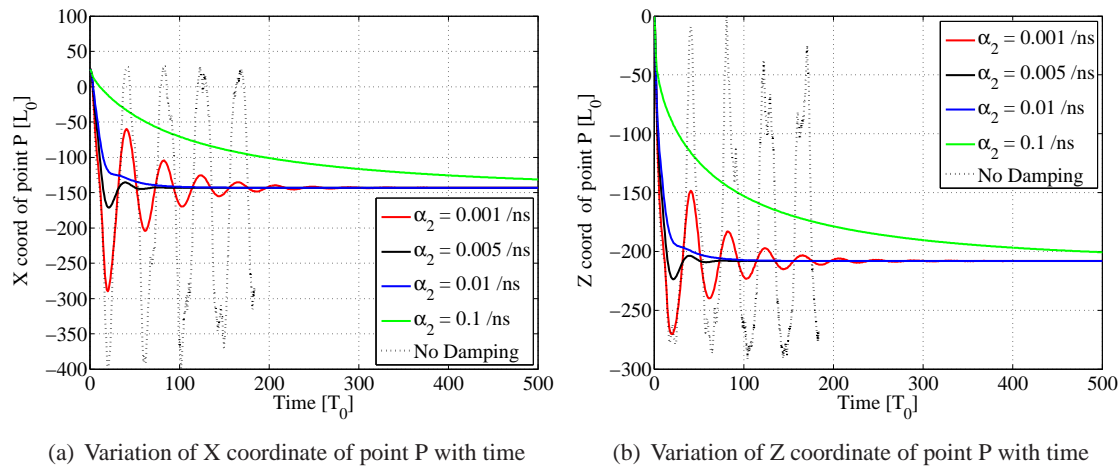
Figure 15: Variation of X and Z coordinate of point P of the spatula for various value of damping parameters. Newmark scheme is used for time discretization. Notice that the Newmark scheme diverges after $t \approx 180T_0$.

Israelachvili, J. N. (1991). *Intermolecular and Surface Forces*. Academic Press, London.

Krenk, S. (2006). Energy conservation in newmark based time integration algorithms. *Comput. Meth. Appl. Mech. Eng.*, 195:6110–6124.

Krenk, S. (2009). *Non-linear Modeling and Analysis of Solids and Structures*. Cambridge University Press, Cambridge.

Krenk, S. and Hogsberg, J. R. (2005). Properties of time integration with first order filter damping. *Int. J. Numer. Methods Eng.*, 64:547–566.

Newmark, N. N. (1959). A method for computation for structural dynamics. *Proc. of the ASCE: J. Eng. Mech. Division*, 85:67–94.

Noh, G., Ham, S., and Bathe, K. J. (2013). Performance of an implicit time integration scheme in the analysis of wave propagations. *Comput. Struct.*, 123:93–105.

Rizzo, N. W., Gardner, K. H., Walls, D. J., Keiper-Hrynko, N. M., Ganzke, T. S., and Hallahan, D. L.

(a) Variation of X coordinate of point P with time

(b) Variation of Z coordinate of point P with time
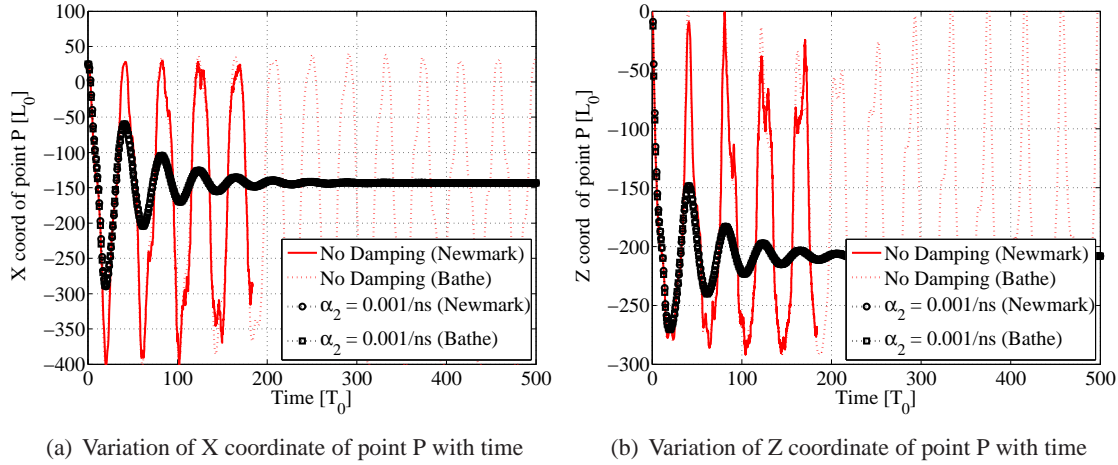
Figure 16: Comparison of variation of X and Z coordinate of point P of the spatula for two value of damping parameters using Newmark and Bathe schemes. Notice that the Newmark scheme diverges after $t \approx 180 T_0$.

(2006). Characterization of the structure and composition of gecko adhesive setae. *J. R. Soc. Interface*, 3:441–451.

Sauer, R. A. (2009). Multiscale modelling and simulation of the deformation and adhesion of a single gecko seta. *Comput. Meth. Biomech. Biomed. Eng.*, 12:627–640.

Sauer, R. A. (2010). A computational model for nanoscale adhesion between deformable solids and its application to gecko adhesion. *J. Adhes. Sci. Technol.*, 24:1807–1818.

Sauer, R. A. (2011). Enriched contact finite elements for stable peeling computations. *Int. J. Numer. Methods Eng.*, 87:593–616.

Sauer, R. A. and Holl, M. (2013). A detailed 3D finite element analysis of the peeling behavior of a gecko spatula. *Comput. Meth. Biomech. Biomed. Eng.*, 16:577–591.

Sauer, R. A. and Li, S. (2008). An atomistically enriched continuum model for nanoscale contact mechanics and its application to contact scaling. *J. Nano. Nanotech.*, 8:3757–3773.

Sauer, R. A. and Lorenzis, L. D. (2013). A computational contact formulation based on surface potentials. *Comput. Meth. Appl. Mech. Eng.*, 253:369–395.

Sauer, R. A. and Wriggers, P. (2009). Formulation and analysis of a 3D finite element implementation for adhesive contact at the nanoscale. *Comput. Meth. Appl. Mech. Eng.*, 198(49-52):3871–3883.

Simo, J. C. and Tarnow, N. (1992). The discrete energy-momentum method. conserving algorithms for nonlinear elastodynamics. *Z. Angew Math. Phys*, 43:757–792.

Sun, W., Neuzil, P., Kustandi, T. S., Oh, S., and Samper, D. (2005). The nature of the gecko lizard adhesive force. *J. Biophys.*, 89:L14–L17.

Wriggers, P. (2008). *Nonlinear Finite Element Methods*. Springer-Verlag, Heidelberg.

Zienkiewicz, O. C. and Taylor, R. L. (2005). *The Finite Element Method for Solid and Structural Mechanics*. Butterworth-Heinemann, Oxford, 6th edition.

(a) $t = 0$ ns   (b) $t = 95$ ns   (c) $t = 150$ ns
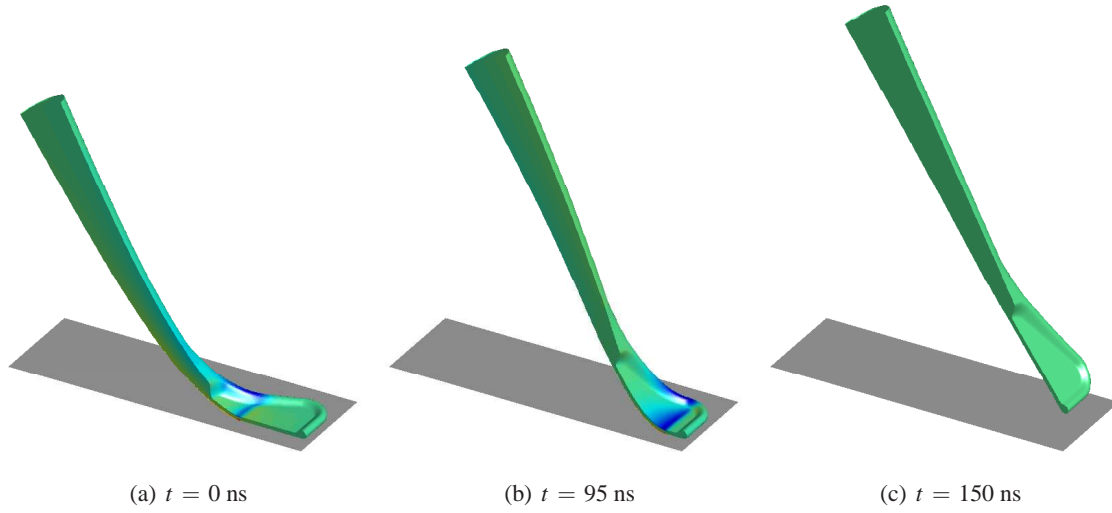
Figure 17: Spatula deformation for an applied vertical displacement $\bar{u}(t)$. The color scale shows the first invariant of stress normalized by Young's modulus E. The value of the color plots ranges from -0.125 E to 0.250 E.

(a) Pull-off force with applied displacement   (b) Zoomed view of figure (a)
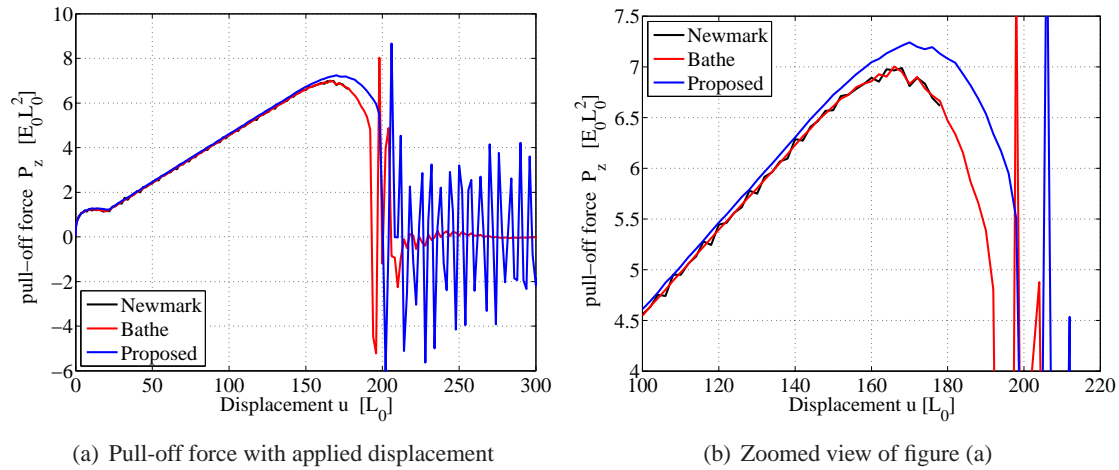
Figure 18: Spatula pull-off force with applied displacement using different schemes. Figure (a) shows the full plot where as figure (b) shows the zoomed view at maximum pull-off force. It should be noted that the Newmark scheme diverges. The spurious oscillations in the response of Newmark scheme are clearly visible in Fig. (b) which are not present for the Bathe composite scheme and the proposed scheme.
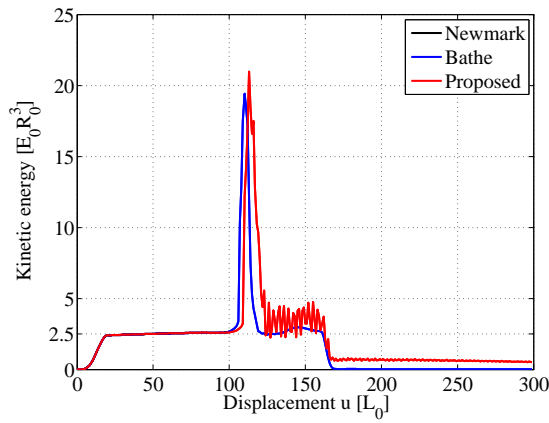
Figure 19: Variation of kinetic energy with time for different schemes. For the case with Bathe composite scheme, the kinetic energy quickly damps out where as for the proposed scheme it decreases slowly .

(a) Computational time per increment

(b) Computational time per increment per NR iteration

(c) Number of NR iterations per increment
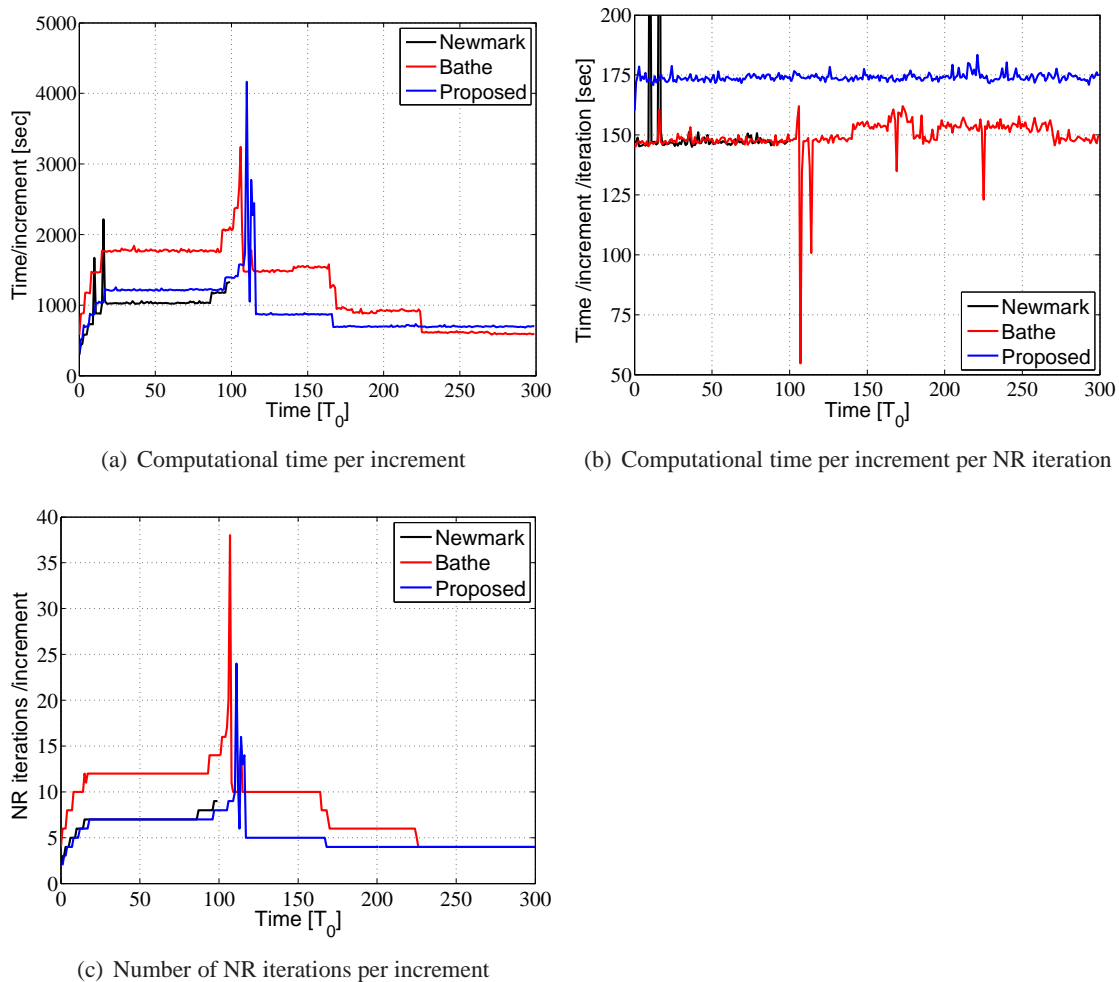
Figure 20: Comparison of computational effort required for simulating the peeling of a gecko spatula using different schemes. It can be seen that the computational effort required using the proposed scheme is lower.